03,09

# High-frequency EPR spectroscopy of $Cr^{3+}$ ions in $\beta$-$Ga_2O_3$ single crystals

© A.S. Gurin[1], D.D. Kramushchenko[1], A.V. Batueva[1], D.A. Bauman[2,¶], D.Yu. Panov[2], A.E. Romanov[1,2], V.A. Spiridonov[2], Yu.A. Uspenskaya[1], H.R. Asatryan[1], R.A. Babunts[1], P.G. Baranov[1]

[1] Ioffe Institute,
St. Petersburg, Russia
[2] ITMO University,
St. Petersburg, Russia
¶ E-mail: dabauman@itmo.ru

Received November 27, 2025
Revised November 27, 2025
Accepted November 28, 2025

Beta-phase gallium oxide ($\beta$-$Ga_2O_3$) bulk single crystals doped with $Cr^{3+}$ ions were investigated by the electron paramagnetic resonance (EPR) at a frequency of 94 GHz (W-band) and a temperature of 6 K. In the EPR spectra of samples with a high concentration of trivalent chromium, in addition to three well-known lines of the $Cr^{3+}$ ($S = 3/2$) in an octahedral oxygen environment, three less intense lines were observed. These signals were attributed to chromium ions in a tetrahedral position based on the analysis of anisotropic EPR spectra and numerical modeling of experimental angular dependences. The fine structure parameters of the spin Hamiltonian, the directions of the magnetic axes and energy level diagram for the ground state of this new center were determined in this paper.

**Keywords:** gallium oxide, electron paramagnetic resonance, impurity centers.

DOI: 10.61011/PSS.2026.01.63235.8808-25

## 1. Introduction

The interest in metal oxide compounds in the modern world is caused by the great possibilities of their use in instrument engineering, and gallium oxide occupies a special among these materials. Its unique properties — large band gap ($E_g = 4.8$ eV), low leakage currents and large permittivity values ($\varepsilon = 10.2-14.2$) — make $\beta$-$Ga_2O_3$ suitable for creating semiconductor devices such as thin-film field-effect transistors, Schottky barriers with reverse voltages up to several kilovolts, and sun-blind UV detectors. High chemical and thermal, as well as radiation resistance, make it possible to use gallium oxide to develop devices designed to operate at elevated temperatures and in the space industry [1–6].

Gallium oxide $Ga_2O_3$ exists in five different crystal modifications — $\alpha$-, $\beta$-, $\gamma$-, $\delta$- and $\varepsilon$-phases, each of which is characterized by a unique crystal lattice structure [7]. Polymorphic compounds of gallium oxide differ not only in space groups, but also in the coordination number of gallium ions. Of particular interest among all phases is the $\beta$-phase of $Ga_2O_3$, the thermodynamically most stable modification that can be obtained from any other polymorphic oxide form by annealing in air at high temperature.

The crystal structure $\beta$-$Ga_2O_3$ is monoclinic with the space group C2/m-$C_{2h}^3$. Lattice parameters at 273 K: $a = 1.223$ nm, $b = 0.304$ nm, $c = 0.580$ nm, $\beta = 104°$. The unit cell contains 4 gallium atoms located in positions like $i$ with local symmetry $m$-$C_2$. The positions of these atoms are crystallographically nonequivalent: two gallium atoms ($Ga_I$) are in an octahedral environment and are coordinated by six oxygen atoms, the other two atoms ($Ga_{II}$) are surrounded by four oxygen atoms, forming a tetrahedral environment [8–10].

Figure 1 shows the structure of the unit cell $\beta$-$Ga_2O_3$, which shows octahedral and tetrahedral positions of gallium surrounded by oxygen atoms. The crystallographic axes are designated as $a$, $a^*$, $b$, $c$. The axis $a^*$ is perpendicular to the plane $(bc)$, and the axis $a$ is deflected from the axis $c$ by an angle 104°.

Transition metal ions can be introduced into the crystal on purpose, or they can form as an uncontrolled impurity during growth due to their presence in the initial matrix. Impurities largely determine the electrical and optical properties of the crystal. Transition metal ions lead to the formation of deep levels in wide-band semiconductors, limiting their electrical conductivity. Currently, these impurities are used to produce semi-insulating materials.

Paramagnetic ions in crystals are an essential element of modern high-tech devices: lasers, masers, oscillators, and quantum sensors. The $Cr^{3+}$ ion occupies a special place, and its introduction into corundum ($Al_2O_3$) has provided a breakthrough in the development of solid-state lasers. Currently, $Cr^{3+}$ is considered as a potential basis for spin qubits in quantum computing [11].

The electron paramagnetic resonance (EPR) method makes it possible to uniquely identify transition metal impurities, their charge state and electronic structure. Unlike the standard bands ($X$- and $Q$-bands) used in most EPR spectrometers, high-frequency spectroscopy ($W$-band) has

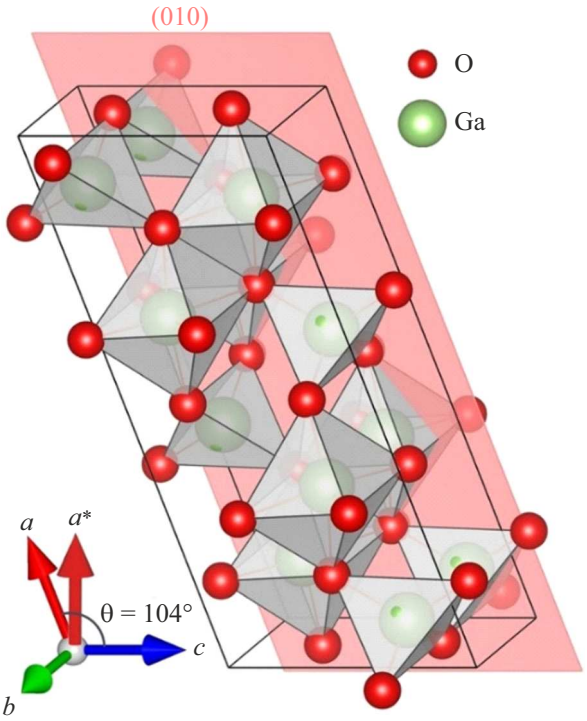


**Figure 1.** The structure of the unit cell of a single crystal $\beta$-$Ga_2O_3$.

a number of significant advantages: high sensitivity, high spectral resolution, and also allows the study of systems with large zero-field splittings of a fine structure.

## 2. Experimental part

Bulk crystals $\beta$-$Ga_2O_3$:Cr were grown by the Czochralski method on an industrial crystal growth setup with induction heating of an iridium crucible. Powdered $Ga_2O_3$ with a purity of 99.999 % (5N) was used as the starting material. $Cr^{3+}$ ions were introduced into the crystal structure intentionally during growth, using metallic chromium flakes with a purity of 99.99 %. Fragments of $\beta$-$Ga_2O_3$ in the form of bars with approximate dimensions $3\times3\times30$ mm, obtained from previously grown crystals, were used as seeds. In the growth process, the previously selected [12] atmospheric composition was used, consisting of a mixture of Ar and $O_2$, the oxygen content was 4–5 vol.%. The growth conditions were as follows: the pressure in the growth chamber was about 1.1 bar, the temperature was about 1850 °C, the rotation speed of the crystal during the growing process was 5 rpm, the pulling speed was about 0.15 mm/min.

Two samples were examined $\beta$-$Ga_2O_3$:Cr with different chromium concentrations: 0.4 mol.% (sample # 1) and 0.5 mol.% (sample # 2). To conduct the experiments, thin plates with dimensions of about $2\times2\times0.5$ mm were cleaved from the central part of each bulk crystal along the cleavage plane (100). The samples were preliminarily oriented by X-ray methods in crystallographic planes. The sample manufacturing technology is described in detail in Ref. [13].

The measurements were performed using an EPR high-frequency spectrometer developed at the Ioffe Institute in collaboration with „DOK“ LLC. The spectrometer, operating in both continuous and pulsed mode, is based on a range of microwave bridges (94 and 130 GHz) and a fully autonomous magneto-optical closed-loop cryogenic system with an operating temperature range of 1.5–300 K and a wide range of magnetic fields (from −7 T to +7 T) [14,15].

Measurements of samples $\beta$-$Ga_2O_3$:Cr was performed in continuous mode at a frequency of 94 GHz using a non-resonator technique [16], at a temperature of 6 K and a magnetic field modulation of 5 G.

## 3. Results and discussion

A number of papers [17–20] previously reported EPR studies of single crystals of $\beta$-$Ga_2O_3$ doped with chromium. The article [21] also presents the results of an EPR study of nominally undoped commercial bulk crystals $\beta$-$Ga_2O_3$. In all these studies, the spectra of the chromium ion were observed exclusively in the octahedral position in the charge state of $Cr^{3+}$. The electron spin of the $Cr^{3+}$ ion is equal to $S = 3/2$ (electronic configuration $3d^3$, ground multiplet $^4F_{3/2}$). Therefore, three lines are observed in the EPR spectra. The authors of the publication [22] determined the magnetic axes of the chromium octahedral center in $\beta$-$Ga_2O_3$. It should be noted that EPR signals from two magnetically nonequivalent centers were observed in studies of $\beta$-$Ga_2O_3$ doped with iron: $Fe^{3+}$ ions in both octahedral and tetrahedral positions [23,24].

Figure 2 shows the orientation dependence of the EPR signals of the $Cr^{3+}$ ion for a sample # 1 with a low chromium concentration recorded in continuous-wave mode at a frequency of 94 GHz at a temperature of 6 K and rotation of the sample in the plane $(ca^*)$ in increments of 10°. $Cr^{3+}$ ions replace gallium and occupy octahedral positions in the lattice $\beta$-$Ga_2O_3$, calculated dependences are shown in red lines in Figure 2. Signals from the paramagnetic center $Cr^{3+}$ are observed in magnetic fields up to 2.3 T which are associated with forbidden $\Delta m_s = \pm2$ transitions, they are indicated in Figure 2 by dotted lines.

An abbreviated spin Hamiltonian in the standard form was used to describe the EPR spectra of $Cr^{3+}$ ions shown in Figure 2:

$$H = \mu_B \mathbf{B}\cdot g\mathbf{S} + D\left[S_z^2 - (S(S+1))/3\right] + E[S_x^2 - S_y^2], \quad (1)$$

where spin $S = 3/2$ for $Cr^{3+}$. The first term describes the Zeeman interaction with the anisotropic $g$-factor, where $\mu_B$ is the Bohr magneton. The second and third terms describe the fine-structure interaction, which leads the splitting of energy levels in a zero magnetic field. The parameter $D$ takes into account the contribution of the $z$-axial part of the crystal field, and the parameter $E$ takes

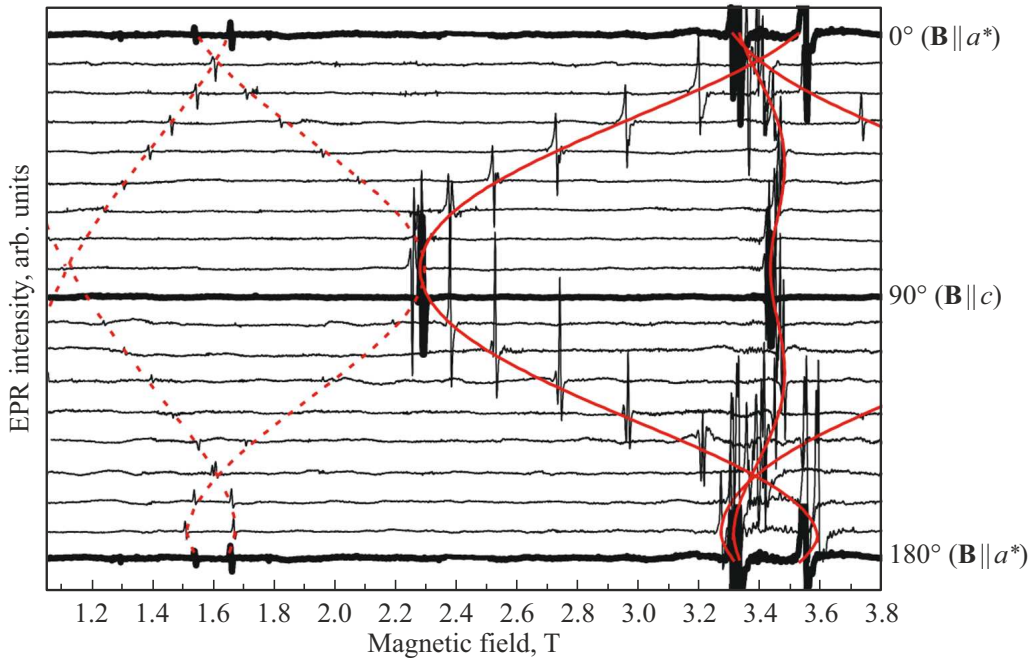


**Figure 2.** Angular dependences of the EPR spectra of chromium ions in $\beta$-$Ga_2O_3$ (sample #1). The spectra were recorded in the plane $(ca^*)$ at a temperature of 6 K and at a frequency of 94 GHz. The calculated dependencies are shown in red lines, the dotted line indicates the forbidden $\Delta m_s = \pm 2$ transitions.

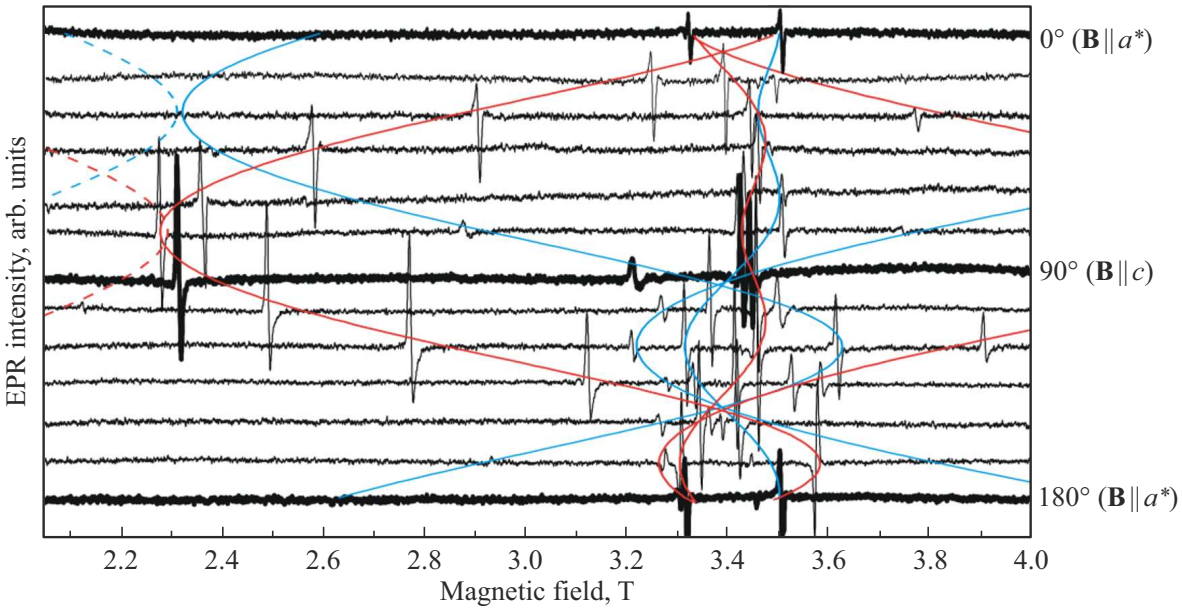


**Figure 3.** Angular dependences of the EPR spectra of chromium ions in $\beta$-$Ga_2O_3$ (sample #2). The spectra were recorded in the plane $(ca^*)$ at a temperature of 6 K and at a frequency of 94 GHz. The calculated angular dependencies for the octahedral position of chromium are indicated by a red line, and for the tetrahedral position by a blue line. Forbidden transitions from the paramagnetic center $Cr^{3+}$ to $\Delta m_s = \pm 2$ are marked with dotted lines.

into account the contribution of the non-axial part. The EPR spectra of $Cr^{3+}$ ions in octahedral positions were calculated using the Grachev program [25], which is based on an accurate numerical diagonalization of the spin Hamiltonian matrix. The parameters of the spin Hamiltonian from Ref. [17] were used as a basis: $g_x = 1.969$, $g_y = 1.964$, $g_z = 1.940$, $|D| = 16025$ MHz, $E = 3860$ MHz.

The orientation dependences shown in Figure 3 were obtained for the sample #2 with an increased chromium concentration. The measurements were performed in

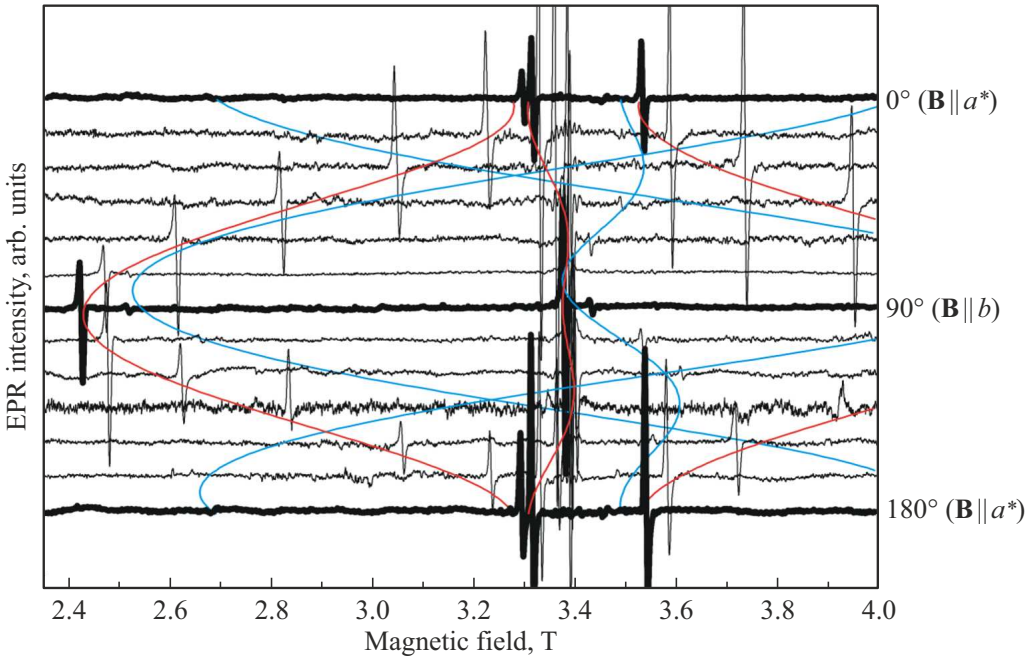


**Figure 4.** Angular dependences of the EPR spectra of chromium ions in $\beta$-$Ga_2O_3$ (sample #2). The spectra were recorded in the plane $(ba^*)$ at a temperature of 6 K and at a frequency of 94 GHz. The red line corresponds to the calculated angular dependencies for chromium in the octahedral position, the blue line corresponds to the calculated angular dependencies for chromium in the tetrahedral position.

continuous mode at a frequency of 94 GHz at a temperature of 6 K and rotation of the sample in the plane $(ca^*)$ in increments of 15°. In addition to the previously well-studied signals related to the octahedral center of chromium, the angular dependences of less intense signals were observed for the first time. An analysis of the calculated parameters allowed us to conclude that these signals belong to chromium ions located in tetrahedral lattice sites. Red lines in Figure 3 correspond to the calculated angular dependences for chromium ions in the octahedral position, and the blue lines correspond to the calculated angular dependences for chromium ions in the tetrahedral position.

The angular dependences of the EPR spectra of $Cr^{3+}$ ions for the sample $\beta$-$Ga_2O_3$ with increased chromium concentration were also recorded in the plane $(ba^*)$ (Figure 4). The measurements were carried out in continuous mode at a frequency of 94 GHz at a temperature of 6 K and rotation of the sample in the plane $(ca^*)$ in increments of 15°. The red and blue curves reflect the calculated angular dependencies, taking into account the sample orientation error of 4° during the experiment. As in the plane $(ca^*)$, two groups of lines are clearly visible here: the red lines correspond to chromium in the octahedral position, and the blue lines correspond to chromium in the tetrahedral position.

The observed angular dependences of the EPR spectra of the tetrahedral position of chromium are well described by the spin Hamiltonian (1) with the following parameters obtained from experimental data: $g_x = 1.969$, $g_y = 1.964$, $g_z = 1.940$, $|D| = 15740$ MHz, $E = 3350$ MHz. From the angular dependences shown in Figure 3, it is established that the magnetic axes of the tetrahedral chromium center are rotated relative to the octahedral one by an angle of 46° around the axis $b$ in the plane $(ca^*)$.

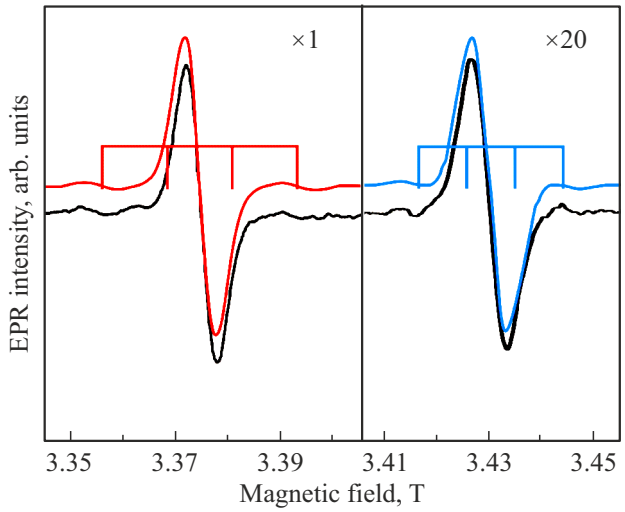


**Figure 5.** Fragment of the EPR spectrum of the chromium isotope $^{53}Cr$ in the $Ga_2O_3$:Cr sample. The spectrum was recorded in the plane $(ba^*)$ at a temperature of 6 K and at a frequency of 94 GHz. The simulated signal is shown by red color for the octahedral position of chromium, and blue color shows the tetrahedral position with an amplification of 20, times.

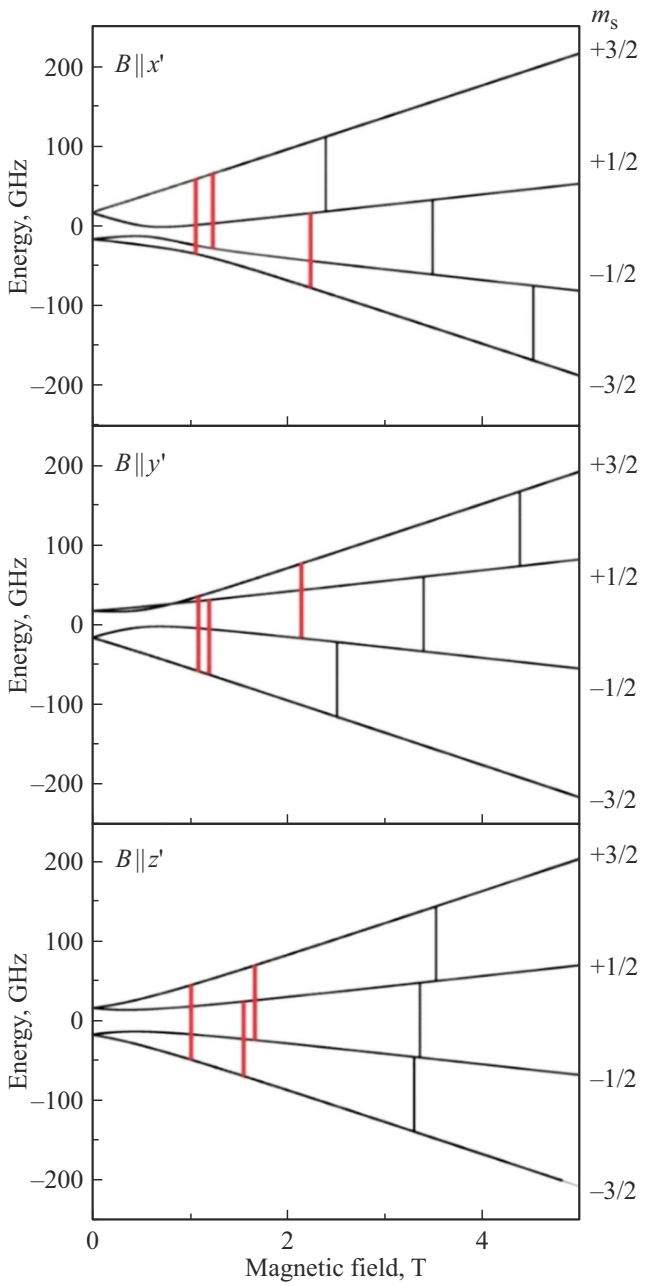


**Figure 6.** Diagram of the energy levels of the ground state of $Cr^{3+}$ ions in a tetrahedral oxygen environment in $\beta$-$Ga_2O_3$ indicating the EPR transitions corresponding to *W*-band. The allowed EPR transitions are marked with black vertical lines, and the forbidden ones are marked with red lines.

An enlarged fragment of the EPR spectrum of the $Ga_2O_3$:Cr sample is shown in Figure 5 registered in the plane $(ba^*)$ at orientation B $\parallel$ *b*. Intense lines and four equidistant lines of lower intensity superimposed on them are observed. Since in addition to the even isotopes of chromium with nuclear spin equal to zero ($I = 0$), there is also the odd isotope $^{53}Cr$ with spin $I = 3/2$, this suggests the presence of 4 lines in the hyperfine structure (HFS). However, due to the width of the main isotope line, only

**Table.** Angle values for the magnetic axes of the octahedral $(x, y, z)$ and tetrahedral $(x', y', z')$ positions $Cr^{3+}$ in $\beta$-$Ga_2O_3$ in a spherical coordinate system

| Octahedral position of ion $Cr^{3+}$ in $\beta$-$Ga_2O_3$ | | | Tetrahedral position of ion $Cr^{3+}$ in $\beta$-$Ga_2O_3$ | | |
|---|---|---|---|---|---|
| | $\theta$, ° | $\phi$, ° | | $\theta'$, ° | $\phi'$, ° |
| $x$ | 72.5 | 0 | $x'$ | 118.5 | 0 |
| $y$ | 90 | 90 | $y'$ | 90 | 90 |
| $z$ | 17.5 | −180 | $z'$ | 28.5 | 0 |

the extreme lines of the chromium HFS are observed. The central intense line is caused by the even isotope of chromium, and the low-intensity lines represent the components of the magnetic HFS of the odd isotope. The ratio of the intensities of the observed lines in the EPR spectrum corresponds to the natural abundance of chromium isotopes. Figure 5 shows the simulated signals: red corresponds to the octahedral position of chromium, blue corresponds to the tetrahedral position. When calculating the shape of the line, the following parameters were used: for chromium in an octahedral oxygen environment — the hyperfine structure constant $A = 125$ G and the line width 60 G; for the tetrahedral position of chromium — $A = 90$ G and the line width is 67 G. The EPR signals shown in Figure 5

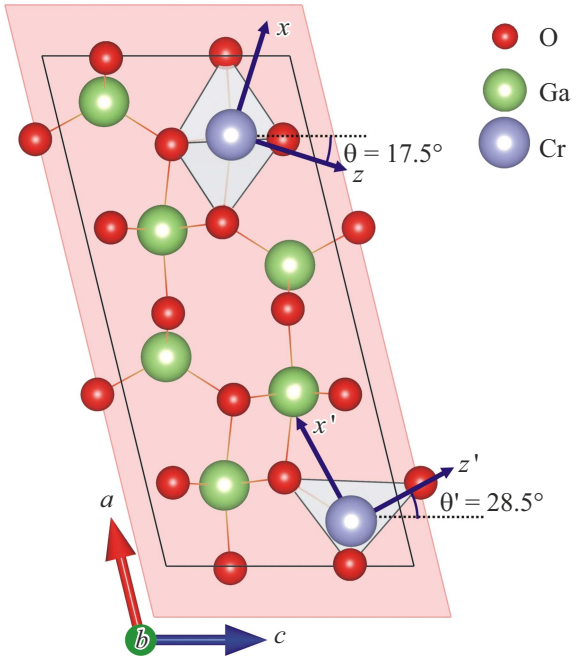


**Figure 7.** Projection of the unit cell $\beta$-$Ga_2O_3$ onto the plane (010). The purple arrows indicate the directions of the magnetic axes of the $Cr^{3+}$ ions for the octahedral and tetrahedral positions. The values of the angles between the magnetic and crystallographic axes are shown in the table.

fully correspond to those expected for $Cr^{3+}$ ions in two nonequivalent positions.

Figure 6 shows the energy-level splitting diagram for the ground state of chromium in a tetrahedral position for three directions of the magnetic axes $x'$, $y'$, $z'$. The calculation is performed using the parameters of the spin Hamiltonian (1). Vertical lines in the diagram indicate EPR transitions for the $Cr^{3+}$ ion in a tetrahedral oxygen environment at a frequency of 94 GHz: the black lines correspond to allowed transitions, and the red lines correspond to forbidden transitions.

The crystal structure of $\beta$-$Ga_2O_3$ was modeled using the Vesta XTalDraw program [26]. Figure 7 shows its projection onto the plane (010), indicating the directions of the magnetic axes for the two chromium positions, which were obtained as a result of calculations (Table). The angles for the magnetic axes of the octahedral $(\theta, \varphi)$ and tetrahedral $(\theta', \varphi')$ positions $Cr^{3+}$ in $\beta$-$Ga_2O_3$ are given in a spherical coordinate system. It should be noted that the directions of the magnetic axes for the octahedral chromium center completely coincide with the data from Ref. [22], and for the tetrahedral position $Cr^{3+}$ these directions were determined for the first time in the framework of this study.

## 4. Conclusion

Studies of chromium-doped single crystals $\beta$-$Ga_2O_3$ by the EPR method in the $W$-band have shown that chromium first replaces energetically more favorable positions of ions $Ga_I^{3+}$ in an octahedral oxygen environment. As the concentration increases, chromium also occupies tetrahedral positions $Ga_{II}^{3+}$. This is due to the difference in ionic radii: for the octahedral position $Ga_I^{3+}$ , the radius is 0.062 nm, whereas it is significantly smaller for the tetrahedral position $Ga_{II}^{3+}$— 0.0477 nm [17].

Based on the analysis of anisotropic spectra and numerical modeling, the parameters of the spin Hamiltonian are calculated, and the directions of the magnetic axes for chromium in the tetrahedral position are determined. According to the crystal structure modeling data, the magnetic axis $z'$ of the tetrahedral chromium center coincides with the direction of one of the Ga-O bonds, which is consistent with the calculations of the directions of the magnetic axes for this center.

### Acknowledgments

The authors would like to thank Valery Y. Davydov for fruitful cooperation and valuable consultations.

### Funding

Experimental studies and calculations were carried out by A.S. Gurin, D.D. Kramushchenko, A.V. Batueva, Yu.A. Uspenskaya and R.A. Babunts within the framework of the state assignment of the Ministry of Science and Higher Education of the Russian Federation (subject No. FFUG–2024–0046). The growth and preparation of samples were carried out by D.A. Bauman, D.Y. Panov, A.E. Romanov and V.A. Spiridonov under a grant from the Russian Science Foundation (grant No. 24-12-00229).

### Conflict of interest

The authors declare that they have no conflict of interest.

## References

[1] S.I. Stepanov, V.E. Nikolaev, V.E. Bougrov, A.E. Romanov, Rev. Adv. Mater. Sci. **44**, 63 (2016).
[2] S.J. Pearton, J. Yang, P.H. Cary IV, F. Ren, J. Kim, M.J. Tadjer, M.A. Mastro. Appl. Phys. Rev. **5**, 011301 (2018).
[3] M. Higashiwaki, G.H. Jessen. Appl. Phys. Lett. **112**, 060401 (2018).
[4] J. Kim, S.J. Pearton, C. Fares, J. Yang, F. Ren, S. Kima, A.Y. Polyakov. J. Mater. Chem. C **7**, 10 (2019).
[5] S.J. Pearton, A. Aitkaliyeva, M. Xian, F. Ren, A. Khachatrian, A. Ildefonso, Z. Islam, M.A. Jafar Rasel, A. Haque, A.Y. Polyakov, J. Kim. ECS J. Solid State Sci. Technol. **10**, 055008 (2021).
[6] D.A. Bauman, A.I. Borodkin, A.A. Petrenko, D.I. Panov, A.V. Kremleva, V.A. Spiridonov, D.A. Zakgeim, M.V. Silnikov, M.A. Odnoblyudov, A.E. Romanov, V.E. Bougrov. Acta Astronautica **180**, 125 (2021).
[7] X.T. Zhou, F. Heigl. Phys. Rev. **75**, 125303 (2007).
[8] S. Geller. J. Chem. Phys. **33**, 676 (1960).
[9] J. Ahman, G. Svensson, J. Albertsson. Acta Crystallogr. C **52**, 1336 (1996).
[10] J.E. Hogan, S.W. Kaun, E. Ahmadi, Y. Oshima, J.S. Speck. Semicond. Sci. Technol. **31**, *6*, 065006 (2016).
[11] V.K. Sewani, R.J. Stöhr, R. Kolesov, H.H. Vallabhapurapu, T. Simmet, A. Morello, A. Laucht. Phys. Rev. B **102**, *10*, 104114 (2020).
[12] D.A. Zakgeim, D.I. Panov, V.A. Spiridonov, A.V. Kremleva, A.M. Smirnov, D.A. Bauman, V.E. Bougrov. Tech. Phys. Lett. **46**, *11*, 1144 (2020).
[13] D.A. Bauman, D.I. Panov, D.A. Zakgeim, V.A. Spiridonov, A.V. Kremleva, A.A. Petrenko, P.N. Brunkov, N.D. Prasolov, A.V. Nashchekin, A.M. Smirnov, M.A. Odnoblyudov, V.E. Bougrov, A.E. Romanov. Phys. Status Solidi A **218**, *20*, 2100335 (2021).
[14] E.V. Edinach, Y.A. Uspenskaya, A.S. Gurin, R.A. Babunts, H.R. Asatryan, N.G. Romanov, A.G. Badalyan, P.G. Baranov. Phys. Rev. B **100**, 104435 (2019).
[15] R.A. Babunts, A.G. Badalyan, A.S. Gurin, N.G. Romanov, P.G. Baranov, A.V. Nalivkin, L.Yu. Bogdanov, D.O. Korneev. Appl. Magn. Reson. **51**, 1125 (2020).
[16] R.A. Babunts, A.G. Badalyan, N.G. Romanov, A.S. Gurin, D.O. Tolmachev, P.G. Baranov. Tech. Phys. Lett. **38**, 887 (2012).
[17] T.H. Yeom, I.G. Kim, S.H. Lee, S.H. Choh, Y.M. Yu. J. Appl. Phys. **93**, *6*, 3315 (2003).
[18] J.E. Stehr, M. Jansson, D.M. Hofmann, J. Kim, S.. Pearton, W.M. Chen, I.A. Buyanova. Appl. Phys. Lett. **119**, 052101 (2021).

[19] H.H. Tippins. Phys. Rev. **137**, *3A*, A865 (1965).
[20] M. Peter and A.L. Schawlow. Bull. Amer. Phys. Soc., Ser. II **5**, 158 (1960).
[21] R.A. Babunts, A.S. Gurin, E.V. Edinach, H.J. Drouhin, V.I. Safarov, P.G. Baranov. J. Appl. Phys. **132**, 155703 (2022).
[22] W. Gunsser, K. Rohwer. Phys. Stat. Sol. (b) **116**, 275 (1983).
[23] R. Buscher, G. Lehmann. Z. Naturforsch **42a**, 67 (1987).
[24] D. Toloman, A. Popa, M. Stan, T.D. Silipas, A.R. Biris. AIP Conference Proceedins **1700**, 060005 (2015).
[25] V.G. Grachev. JETP **65**, *5*, 1029 (1987).
[26] K. Momma, F. Izumi. J. Appl. Cryst. **44**, 1272 (2011).

*Translated by A.Akhtyamov*